J|A|C|S
ARTICLES
Published on Web 06/15/2004

Planar Nets of Ti Atoms Comprising Squares and Rhombs in the New Binary Antimonide Ti_2Sb

Shahab Derakhshan,[†] Abdeljalil Assoud,[†] Katja M. Kleinke,[†] Enkhtsetseg Dashjav,[†] Xiangyun Qiu,[‡] Simon J. L. Billinge,[‡] and Holger Kleinke*,[†]

Contribution from the Department of Chemistry, University of Waterloo, Waterloo, ON, Canada N2L 3G1, and Department of Physics and Astronomy, Michigan State University, East Lansing, Michigan 48824

Received March 26, 2004; E-mail: kleinke@uwaterloo.ca

Abstract: The new binary antimonide Ti_2Sb was found to crystallize in a distorted variant of the La_2Sb type, which contains a square planar La net with short La−La bonds. In the Ti_2Sb structure, the corresponding Ti net is deformed to squares and rhombs in order to enhance Ti−Ti bonding, as proven by single-crystal X-ray investigation in combination with the real-space pair distribution function technique utilizing both X-ray and neutron powder diffraction data. Electronic structure calculations revealed a lowering of the total energy caused by the disorder, the major driving force being strengthened Ti−Ti interactions along the diagonal of the Ti_4 rhombs.

Introduction

Infinite planar square nets are found in a number of antimonides, usually formed by the main group elements (here: antimony atoms), e.g., in the ZrSiS type (a polyanionic variant of the PbFCl type),[1−3] $HfCuSi_2$ type,[4−9] and $SmSb_2$ type.[10] Less common types with Sb square nets include $LnGaSb_2$ (Ln = rare earth element)[11] and $LnMSb_3$ (M = transition metal).[12,13] Such square nets of main group elements comprise an ideal valence-electron count of six, e.g., formal Sb^- atoms, with four so-called half bonds per atom.[14,15] These nets are susceptible to a Peierls distortion,[16] which may result in the formation of either cis-trans chains (realized in the structure of GdPS with two single bonds per P atom)[17] or zigzag chains (realized in CeAsS with two As−As single bonds).[18] More complicated distortions are not uncommon, and may lead to incommensurate superstructures, e.g., in tellurides,[19] or to large commensurate superstructures, e.g., Gd_8Se_{15}, a 24-fold superstructure of the ZrSiS type,[20] and GdS_{2-x}, a 144-fold superstructure.[21]

In contrast to the main group examples, square nets of transition metal elements are not prone to distortions. They occur in numerous intermetallic compounds, like $BaAl_4$ and its several derivatives,[22−24] as well as in the structures of the elements, the simplest example being the α-Polonium type. In the more common, closest packed structures (cubic and hexagonal) and the cubic body-centered packing, square nets of metal atoms exist as well, but they only participate in secondary metal−metal bonding. Square nets formed by valence-electron poor transition metals are present in the metal-rich antimonides such as Zr_2Sb[25] (La_2Sb type)[26] and Sc_2Sb[27] (Cu_2Sb/Fe_2As type, *anti*-ZrSiS type). The metal−metal bonds of the square nets are often shorter than in the elements themselves.

The new binary antimonide Ti_2Sb was uncovered during attempts to further verify the usefulness of the Kleinke−Harbrecht structure map of the M_2Q pnictides and chalcogenides.[28] This map was previously utilized to correctly predict

[†] University of Waterloo.
[‡] Michigan State University.

(1) Ferro, R. *Accad. Lincei.* **1952**, *13*, 151−157.
(2) Ferro, R. *Acta Crystallogr.* **1956**, *9*, 817−818.
(3) Hulliger, F. *J. Less-Comm. Met.* **1968**, *16*, 113−117.
(4) Cordier, G.; Schäfer, H.; Woll, P. *Z. Kristallogr.* **1985**, *40B*, 1097−1099.
(5) Leithe-Jasper, A.; Rogl, P. *J. Alloys Compd.* **1994**, *203*, 133−136.
(6) Sologub, O.; Hiebl, K.; Rogl, P.; Noël, H.; Bodak, O. *J. Alloys Compd.* **1994**, *210*, 153−157.
(7) Wollesen, P.; Jeitschko, W.; Brylak, M.; Dietrich, L. *J. Alloys Compd.* **1996**, *245*, L5−L8.
(8) Albering, J. H.; Jeitschko, W. *Z. Naturforsch.* **1996**, *51B*, 257−262.
(9) Myers, K. D.; Bud'ko, S. L.; Fisher, I. R.; Islam, Z.; Kleinke, H.; Lacerda, A. H.; Canfield, P. C. *J. Magn. Magn. Mater.* **1999**, *205*, 27−52.
(10) Wang, R.; Steinfink, H. *Inorg. Chem.* **1967**, *6*, 1685−1692.
(11) Mills, A. M.; Mar, A. *J. Am. Chem. Soc.* **2001**, *123*, 1151−1158.
(12) Brylak, M.; Jeitschko, W. *Z. Naturforsch.* **1995**, *50B*, 899−904.
(13) Ferguson, M. J.; Hushagen, R. W.; Mar, A. *J. Alloys Compd.* **1997**, *249*, 191−198.
(14) Tremel, W.; Hoffmann, R. *J. Am. Chem. Soc.* **1987**, *109*, 124−140.
(15) Papoian, G. A.; Hoffmann, R. *Angew. Chem., Int. Ed.* **2000**, *39*, 2408−2448.
(16) Peierls, R. E. *Quantum Theory of Solids*; Clarendon Press: Oxford, UK, 1955.
(17) Hulliger, F.; Schmelczer, R.; Schwarzenbach, D. *J. Solid State Chem.* **1977**, *21*, 371−374.
(18) Ceolin, R.; Rodier, N.; Khodadad, P. *J. Less-Comm. Met.* **1977**, *53*, 137−140.
(19) Patschke, R.; Kanatzidis, M. G. *Phys. Chem. Chem. Phys.* **2002**, *4*, 3266−3281.
(20) Dashjav, E.; Oeckler, O.; Doert, T.; Mattausch, H.; Böttcher, P. *Angew. Chem., Int. Ed.* **2000**, *39*, 1987−1988.
(21) Tamazyan, R.; Smaalen, S. v.; Vasilyeva, I. G.; Arnold, H. *Acta Crystallogr.* **2003**, *B47*, 709−719.
(22) Parthe, E.; Chabot, B.; Braun, H. F.; Engel, N. *Acta Crystallogr.* **1983**, *B39*, 588−595.
(23) Hulliger, F. *Helv. Phys. Acta* **1985**, *58*, 216−225.
(24) Häussermann, U.; Amerioun, S.; Eriksson, L.; Lee, C.-S.; Miller, G. J. *J. Am. Chem. Soc.* **2002**, *124*, 4371−4383.
(25) Garcia, E.; Corbett, J. D. *J. Solid State Chem.* **1988**, *73*, 440−451.
(26) Stassen, W. N.; Sato, M.; Calvert, L. D. *Acta Crystallogr.* **1970**, *B26*, 1534−1540.
(27) Berger, R. *Acta Chem Scand.* **1977**, *31A*, 514−516.
(28) Kleinke, H.; Harbrecht, B. *Z. Anorg. Allg. Chem.* **2000**, *626*, 1851−1853.

the hitherto uncovered arsenides ZrTiAs and ZrVAs that exhibit undistorted Ti and V square nets, respectively,[29,30] both falling into the La_2Sb domain. Our latest examples were a series of isoelectronic Hf phosphides and arsenides occurring in the Co_2Si region, that do not consist of square nets.[31]

Ti_2Sb would be placed on the border between the La_2Sb and the Cu_2Sb domains in this structure map, and—as presented within this contribution—it actually forms a distorted variant of the former, thereby strictly speaking a new structure type. The unprecedented distortion of the square net is of particular interest, for it optimizes Ti−Ti bonding by shortening the diagonals of every other square, while maintaining the rest as ideal squares. Since no long-range order was detectable, we employed the real-space pair distribution function[32] to experimentally verify the existence of the interatomic distances as postulated in our distorted structure model.

Experimental Section

Synthesis. High temperatures (above 1000 °C) are required to synthesize the metal-rich antimonide Ti_2Sb. This inhibits the use of elemental antimony in the final reaction step because of its high vapor pressure and reactivity at these temperatures. Therefore, we first prepared 10 mmol of $TiSb_2$ by placing the elements Ti and Sb (in powder form, ALFA Aesar, nominal purities > 99.5%) in the stoichiometric ratio of 1:2 into an evacuated fused silica tube, which was then heated in a resistance furnace at 650 °C over a period of 4 days. Next, 1 mmol $TiSb_2$ was thoroughly mixed with 3 mmol Ti, and pressed into a pellet. The pellet was arc-melted once and then again after inversion on a water-cooled copper block under a flow of Argon. The weight loss during arc-melting was negligible, so that no excess of Sb was needed to obtain Ti_2Sb in quantitative yields. To enhance crystallinity, we put the sample into a tantalum crucible, which was sealed under Argon and then placed into a resistance furnace. Therein, the Ti_2Sb sample in the Ta crucible was annealed at 1100 °C over a period of one week, under dynamic vacuum generated by an oil diffusion pump, followed by controlled cooling at a rate of 2 °C/minute to room temperature. The arc-melting step may be skipped, but this typically leads to an inhomogeneous product, requiring grinding and reheating to achieve homogeneity. The successful annealing shows that Ti_2Sb is stable with respect to disproportionation into the neighboring antimonides Ti_3Sb[27] and Ti_5Sb_3[33] over a wide temperature range.

Analysis. Initial analyses were carried out employing an X-ray powder diffractometer with position-sensitive detector (INEL). The pattern obtained after arc-melting showed strong resemblance to that of Zr_2Sb. Therefore, we simulated the Ti_2Sb powder diagram using a model with the positional parameters taken from Zr_2Sb, but with the Ti scattering factors and shrunk lattice parameters, i.e., from $a = 4.11$ Å in Zr_2Sb to 4.00 Å, and from $c = 15.79$ Å to 14.50 Å (retaining the tetragonal body-centered symmetry). The resulting simulation matched the experimental powder diagram well, indicating that we might have prepared the new antimonide Ti_2Sb in the La_2Sb type. The powder diagram of the product did not change after annealing the latter at 1150 °C. No superstructure reflections were visible; all reflections could be indexed based on the small tetragonal unit cell. Rietveld refinements of the Ti_2Sb structure in the La_2Sb type revealed a problematic, i.e., enlarged, isotropic thermal displacement parameter for Ti2, the atom in the square planes (0.05 Å^2 for Ti2 vs 0.02 Å^2 for Ti1).

Subsequent EDS analyses (LEO 1530, with integrated EDAX Pegasus 1200) did not reveal any incorporation of impurity elements, such as oxygen or silicon stemming from the silica tube or tantalum from the Ta crucible. The Ti: Sb ratios of several selected crystals were constantly 67: (33 ± 1) at.-%.

Single-Crystal Structure. A black block-shaped crystal of the dimensions 35 × 27 × 16 μm from a Ti_2Sb sample annealed at 1150 °C was mounted for a room-temperature data collection on a Smart Apex CCD (BRUKER), which utilizes graphite-monochromatized Mo Kα radiation. The crystal-to-detector distance was 4.547 cm. Data were collected by scans of 0.3° in ω, for an overall of 606 frames at $\phi = 0°$. The exposure time was 120 s per frame. The data were corrected for Lorentz and polarization effects. Absorption corrections were based on fitting a function to the empirical transmission surface as sampled by multiple equivalent measurements.[34] Diffraction peaks obtained from all frames of the reciprocal space images were used to determine the unit cell parameters, which indicated tetragonal body-centered symmetry, in accord with the *I*4/*mmm* space group of La_2Sb. Since the structure refinements[35] based on this type revealed anomalous thermal displacement parameters of the Ti site that forms the square planes (Ti2), the data collection was repeated at 150 K.

We commenced the structure refinements of the latter measurement from the atomic parameters of the La_2Sb type in the *I*4/*mmm* space group. The refinements converged smoothly to almost satisfying residual factors, e.g., R1 = 0.055 for all data, but showed unacceptable thermal parameters again for Ti2 only. In this model, Ti2 is located on the *4c* position without any free positional parameter, i.e., fixed on 0, 1/2, 0. We obtained a huge U_{11} parameter of 0.125(7), drastically enlarged compared to $U_{22} = 0.006(1)$ and $U_{33} = 0.003(1)$, yielding $U_{eq} = 0.045(2)$ (all U values given in Å^2). The U values of Ti1 were inconspicuous, with no strong anisotropy and a normal U_{eq} value of 0.0074(7) Å^2. Refining the occupancy factor of Ti2 did not result in a significant deviation from 100% occupancy.

Next, the possibilities of symmetry reduction or split position were considered. There are two symmetry dependent Ti2 atoms per layer within each unit cell, which are related by the 4-fold rotation axis. Removing this axis resulted in two symmetry independent "Ti2" sites (in space group *Immm*) that both exhibited the same effect in a tentative refinement. It is noteworthy that no superstructure reflections were found, despite the long exposure times—in agreement with our X-ray powder diffraction experiments. Therefore, we did not increase the unit cell; instead we allowed Ti2 to deviate from $x = 0$, and thereby refined the x parameter to become 0.0701(6), which is 0.28 Å away from the original *4c* site. This model yields a split position with an interatomic distance of 0.56 Å, for Ti2 is now on *8j*, slightly off a mirror plane (from site symmetry *mmm* to *m*2*m*). On *8j*, the Ti2 thermal parameters are inconspicuous, and the residual factors of the final refinements significantly improved, e.g. from $R1 = 0.055$ to $R1 = 0.029$ (all data). Crystallographic details of both models are summarized in Table 1, and the atomic coordinates of the split model with Ti2 on *8j* may be found in Table 2.

To investigate whether this distortion depends on the synthesis conditions, we collected two more data sets (at room temperature), one taken directly from arc-melting, i.e., without annealing, and one from a sample that was not arc-melted, but annealed at 1150 °C, followed by slow cooling to room temperature. Both refinements gave the same results, including a split position of Ti2.

Pair Distribution Function Technique. The distorted model with split Ti2 sites ultimately yields different interatomic distances, in particular involving Ti−Ti bonds (Table 3), but also Ti−Sb distances in the second coordination sphere (around 4.9 Å). Experimental proof for the presence of the distances stemming from the split of Ti2 sites

(29) Lee, C.-S.; Dashjav, E.; Kleinke, H. *Chem. Mater.* **2001**, *13*, 4053−4057.
(30) Dashjav, E.; Lee, C.-S.; Kleinke, H. *J. Solid State Chem.* **2002**, *169*, 96−102.
(31) Derakhshan, S.; Dashjav, E.; Kleinke, H. *Eur. J. Inorg. Chem.* **2004**, 1183−1189.
(32) Egami, T.; Billinge, S. J. L. *Underneath the Bragg Peaks: Structural Analysis of Complex Materials*; Pergamon Press Elsevier: Oxford, England, 2003.
(33) Berger, R. *Acta Chem. Scand.* **1977**, *31A*, 889−890.
(34) *SAINT*; Version 4 ed.; Siemens Analytical X-ray Instruments Inc.: Madison, WI., 1995.
(35) Sheldrick, G. M. *SHELXTL*; Version 5.12 ed.; Siemens Analytical X-ray Systems: Madison, WI, 1995.

Table 1. Crystal Data and Structure Refinements for Ti_2Sb

	model with Ti2 on 8j	model with Ti2 on 4c
formula weight	217.55 g/mole	
T	150(2) K	
wavelength	0.71073 Å	
space group	*I*4/*mmm*	
unit cell dimensions	$a = 3.9546(8)$ Å	
	$c = 14.611(3)$ Å	
	$V = 228.49(8)$ Å^3	
Z, density (calculated)	6.324 g/cm^3	
absorption coefficient	18.10 mm^{-1}	
reflections collected	616	
independent reflections	176 [R(int) = 0.0259]	
data/restraints/parameters	176/0/12	176/0/11
goodness-of-fit on F^2	1.026	1.166
final *R* indices [$I > 2\sigma(I)$][a]	$R1 = 0.025$, $wR2 = 0.057$	$R1 = 0.049$, $wR2 = 0.118$
R indices (all data)[a]	$R1 = 0.029$, $wR2 = 0.058$	$R1 = 0.055$, $wR2 = 0.122$
largest diff. peak and hole	1.557 and −2.593 e.Å^{-3}	8.268 and −7.234 e.Å^{-3}

[a] $R1 = \Sigma||F_o| - |F_c||/\Sigma|F_o|$; $wR2 = [\Sigma[w(F_o^2 - F_c^2)^2]/\Sigma[w(F_o^2)^2]]^{1/2}$.

Table 2. Atomic Coordinates and Equivalent Isotropic Displacement Parameters for Ti_2Sb from the Single Crystal Study at 150 K[a]

atom	site	*x*	*y*	*z*	U_{eq}/Å^2	occup.
Ti1	4e	0	0	0.3305(1)	0.0074(4)	1
Ti2	8j	0.0701(6)	1/2	0	0.0067(6)	1/2
Sb	4e	0	0	0.13981(4)	0.0063(2)	1

[a] Corresponding values from the X-ray PDF data (room temperature): z(Ti1) = 0.3307(3), U_{eq}(Ti1) = 0.0073(2) Å^2; x(Ti2) = 0.0708(20), U_{eq}(Ti2) = 0.0069(2) Å^2; z(Sb) = 0.1398(1), U_{eq}(Sb) = 0.0035(1) Å^2; and from neutron PDF data (15 K): z(Ti1) = 0.33069(8), U_{eq}(Ti1) = 0.00273(5) Å^2; x(Ti2) = 0.0711(9), U_{eq}(Ti2) = 0.00359(6) Å^2; z(Sb) = 0.13977(6), U_{eq}(Sb) = 0.00242(3) Å^2.

Table 3. Selected Bond Lengths [Å] and ICOHP [eV/bond] for Ti_2Sb

bond	no.	length[a]	ICOHP[b]	length[c]	ICOHP[d]
Ti1−Sb	1×	2.786(2)	−1.57	2.785(4)	−1.57
Ti1−Sb	4×	2.8298(6)	−1.52	2.8300(8)	−1.52
Ti1−Ti2	2×	3.004(2)	−1.31	3.170(3)	−0.96
Ti1−Ti2	2×	3.349(2)	−0.64	3.170(3)	−0.96
Ti2−Ti2	4×	2.8237(7)	−1.74	2.7963(6)	−1.85
Ti2−Ti2	1×	3.401(1)	−0.75	3.9546(8)	−0.20
Ti2−Ti2	2×	3.993(1)	−0.06	3.9546(8)	−0.06
Ti2−Ti2	1×	4.509(2)	−0.01	3.9546(8)	−0.20
Ti2−Sb	4×	2.8565(6)	−1.51	2.843(1)	−1.53

[a] Bond lengths from the final structure refinements, excluding the unreasonable distances between the disordered Ti2 atoms of 0.555(5) Å and 2.404(3) Å. [b] ICOHP values from the hypothetical ordered superstructure (*Cmca*). [c] Bond lengths from the structure refinements with Ti2 fixed on the *4c* site (undistorted model). [d] ICOHP values from the hypothetical structure with Ti2 fixed on the *4c* site (undistorted model).

was directly obtained utilizing the real-space pair distribution function (PDF) technique. The PDF, *G(r)*, gives the probability of finding pairs of atoms separated by the distance *r*, and thereby comprises peaks corresponding to all discrete interatomic distances. The experimental PDF is a direct Fourier transform of the total scattering structure function *S(Q)*, the corrected, normalized intensity, from powder scattering data given by $G(r) = 2/\pi \int_0^\infty Q[S(Q) - 1]\sin QrdQ$, where *Q* is the magnitude of the scattering vector. Unlike crystallographic techniques, the PDF incorporates both Bragg and diffuse scattering intensities resulting in local structural information.[32] Its high real-space resolution is ensured by measurement of scattering intensities over an extended *Q* range ($Q_{max} \geq 30$ Å^{-1}) using short wavelength X-rays or neutrons.

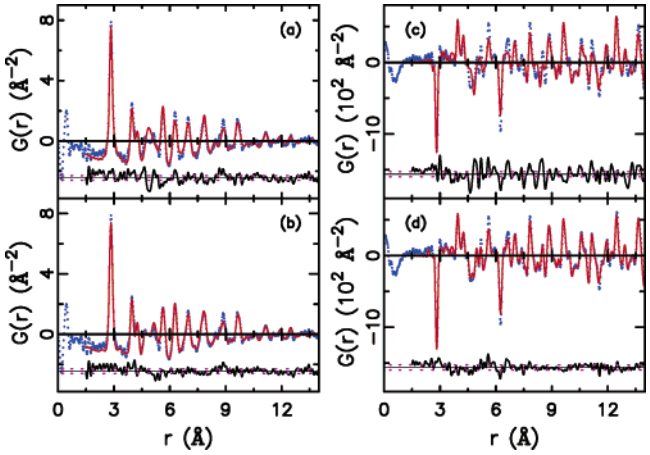

Figure 1. PDFs, *G(r)*. (a), (b): X-ray data; (c), (d): neutron data (shown as the blue dots in both cases). Solid lines are the fits to the model data, with (a) and (c) from the undistorted model and (b) and (d) from the split site model. Difference curves are shown below the data. The dotted lines around the difference curves indicate the standard uncertainties due to random counting statistics on the data at the 1σ level.

Both X-ray and neutron powder diffraction experiments were carried out. These give complementary datasets due to the different relative scattering lengths to neutrons and atomic scattering factors for X-rays of Ti compared to Sb ($f_{Ti}(0)/f_{Sb}(0) = 0.43$ for X-rays vs $b_{Ti}/b_{Sb} = -0.61$ for neutrons). Note that the scattering length of Ti is negative, which explains the minus sign in this equation. This also results in negative Ti−Sb peaks (valleys) in the PDF. Thus, the scattering from Ti, and therefore the PDF peaks originating from Ti correlations, are somewhat more apparent in the neutron data.

The X-ray experiment was performed at the 6-ID beam line at the Advanced Photon Source (APS) at Argonne National Laboratory. A powdered Ti_2Sb sample of disk shape (thickness of 1.0 mm, diameter of 1.0 cm) was loaded into a hollow flat metal plate, and then sealed between thin Kapton films. Data acquisition at 300 K employed the recently developed rapid acquisition PDF (RA-PDF) technique[36] with an X-ray energy of 98.0 keV. A single exposure of the image plate detector was limited to two seconds to avoid detector saturation, and was repeated 20 times to achieve better counting statistics in the high-*Q* region.

The neutron experiment was performed at the newly upgraded neutron powder diffractometer (NPDF) at the Lujan center at Los Alamos National Laboratory.[37] A powdered Ti_2Sb sample of 5.92 g was loaded into a standard 3/8″ vanadium can under helium exchange gas. The sample height was measured to be 2.92 cm. Low temperature is preferred to sharpen the peaks in the PDF, and so data acquisition was carried out at 15 K in a displex closed cycle refrigerator. Data were collected for 10 h. The long collection time was necessitated because of the large amount of incoherent scattering from this sample. Calibration measurements of the background, empty containers, etc., were also performed.

Standard corrections were applied to obtain the total scattering structure functions, *S*(*Q*), using the programs PDFgetX2.0[38] and PDFgetN[39] for X-ray and neutron data, respectively. The resulting PDFs, *G*(*r*), are shown in Figure 1 as the dots, with (a) and (b) showing the X-ray data, and (c) and (d) the neutron data. The data were modeled quantitatively using a real-space profile fitting program, PDFFIT.[40] This program can refine the crystallographic model to the data, in analogy

(36) Chupas, P. J.; Qiu, X.; Hanson, J. C.; Lee, P. L.; Grey, C. P.; Billinge, S. J. L. *J. Appl. Crystallogr.* **2003**, *36*, 1342−1347.
(37) Proffen, T.; Egami, T.; Billinge, S. J. L.; Cheetham, A. K.; Louca, D.; Parise, J. B. *Appl. Phys. Lett.* **2002**, *A74*, S163−S165.
(38) Qiu, X.; Billinge, S. J. L., Unpublished work.
(39) Peterson, P. F.; Gutmann, M.; Proffen, T.; Billinge, S. J. L. *J. Appl. Crystallogr.* **2000**, *33*, 1192.
(40) Proffen, T.; Billinge, S. J. L. *J. Appl. Crystallogr.* **1999**, *32*, 572−575.

with Rietveld refinements. However, local structural distortions can be introduced into the models even when they are not long-range ordered and no crystallographic superstructure reflections are observed as in the current case.

We first fitted the data with the undistorted model, and show the results in Figure 1a (X-ray) and 1c (neutron). Clearly, the undistorted model proves to be insufficient, as evident from the difference curves below the data. Fluctuations significantly larger than the experimental uncertainties (the estimated errors at the 1σ level are shown as dotted lines associated with the difference curves) are observed over the whole fitting range.

One of the strengths of the PDF technique is that it yields quantitatively reliable intermediate range information on nanometer length-scales. The persistence of the fluctuations in the difference curve of Figure 1c are significant and a clear indication that the undistorted model fit to the data is lacking. The effect is less apparent in the X-ray data (Figure 1a) because the measurements were made with much lower *Q*-space resolution, which results in the PDF becoming damped with increasing *r*. The fluctuations in the difference curve are then correspondingly damped.

Next, the distorted model with split Ti2 sites was tried, with the fitting results shown in Figure 1b (X-ray) and 1d (neutron). Compared to the undistorted model, the agreements to both X-ray and neutron PDFs improved significantly over the entire range, with the addition of only one additional refinement parameter, and gave rather satisfactory fits given that the distorted model is an average of the unknown superstructure. The superstructure model in the *Cmca* space group was also tried and gave comparable fits. The structure data from the PDF refined models are in excellent agreement with those refined from the single-crystal X-ray study as shown in Table 2. The full profile PDF refinements confirm that the distorted model describes both the local and average structure to great accuracy and is far superior to the undistorted model. The superstructure model in the *Cmca* space group gives comparable agreement to the split site model, which shows that this model is also consistent with the data as well as making better physical sense.

In addition, the data-PDFs were examined to search for direct evidence of the short and long Ti2−Ti2 distances implicit in the distorted model. A large thermal displacement parameter with no underlying splitting results in broad peaks in the PDF centered on the average position, whereas a split position results in peaks in the PDF splitting into two components that retain their sharpness. Thus, the distorted and undistorted models should be directly distinguishable in the PDF.

Features in the PDF can be compared to expected bond distances from Table 3. The strength of the PDF peak depends on the scattering power of the two atoms contributing to the peak, and the multiplicity of the pair. Since for both X-rays and neutrons Ti is a weaker scatterer than Sb, the low multiplicity Ti−Ti bonds that would show the distortion directly are hard to see. In particular, the Ti1−Ti2 peak centered at 3.17 Å and the Ti2−Ti2 distance at 3.95 Å are barely evident (Figure 2).

There is some suggestion from the neutron data that the 3.17 Å is split (apparent as a highlighted "M"-shaped feature in both the X-ray and neutron difference curves based on the hypothetical undistorted model), but by itself this is hardly convincing. However, the relatively strong Ti2−Sb peak centered at 4.87 Å gives a clear and unequivocal indication of this splitting. The peak from the undistorted model centered at this distance is absent in the experimental data that, instead, have relatively sharp features at 4.65 and 5.10 Å. This results in a clear feature in the difference curves based on the undistorted model below the data in Figure 2. In the X-ray data it is M-shaped and in the neutron data W-shaped. The difference is caused by the change in sign of the Ti−Sb peak in the PDF due to the negative scattering length of Ti. These M/W features clearly show that the peak centered at 4.87 Å has split into a shorter and a longer peak, proving that the distorted model is indeed the correct one.

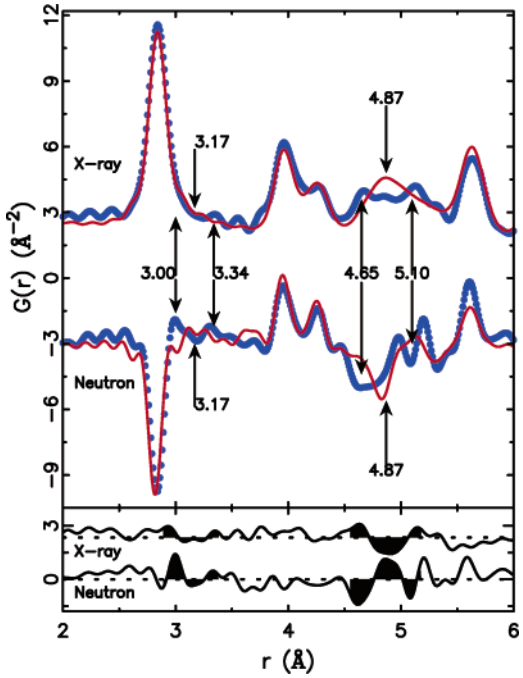

Figure 2. Experimental PDF (blue dots) and the calculated PDF from the hypothetical undistorted model (red line). Upper curves: X-ray data; lower curves: neutron data. The difference curves based on the undistorted model are shown below.

Electronic Structure Calculations. As site deficiencies cannot be directly calculated with our methods, we had to propose an ordered model occurring with exclusively full occupancies. One can postulate ordered superstructures based on the split model that avoid unreasonably short Ti2−Ti2 distances (the split position does not occur with any unrealistic Ti2−Ti1 or Ti2−Sb bonds). The smallest one is a $\sqrt{2} \times \sqrt{2} \times 1$ superstructure in *Cmca* with a pattern of Ti2 rhombs and squares displayed in the right part of Figure 3, compared to the undistorted structure model in the ellipsoid presentation on the left.

We carried out self-consistent tight-binding *first principles* LMTO calculations (LMTO = linear muffin tin orbitals) of the superstructure in *Cmca*, as well as of the undistorted model in *I*4/*mmm*, using the atomic spheres approximation (ASA).[41,42] In the LMTO approach, the density functional theory is used with the local density approximation (LDA).[43] The integration in *k* space was performed by an improved tetrahedron method[44] on a grid of 876 independent *k* points of the first Brillouin zone in the case of the superstructure (and 1131 *k* points in case of the undistorted subcell). The superstructure model is preferred according to the electronic structure calculation, with a lower total energy of 1.3 kJ per mol Ti_2Sb.

Physical Property Measurements. Since no single crystals of sufficient dimensions were available, we pressed part of the ground phase-pure sample into a bar-shaped pellet of the dimensions $5 \times 2 \times 1$ [in mm] for the temperature-dependent electrical resistance measurements using a four-point-method. A self-made device was used to determine the voltage drops ΔV over a distance of 2 mm at a constant current of 10 mA under dynamic vacuum between 295 and 160 K, wherein cooling was achieved by helium compression.

Results and Discussion

Structure Map. We uncovered Ti_2Sb during attempts to clarify the area in the Kleinke-Harbrecht structure map between

(41) Andersen, O. K. *Phys. Rev.* **1975**, *B12*, 3060−3083.
(42) Skriver, H. L. *The LMTO Method*; Springer: Berlin, Germany, 1984.
(43) Hedin, L.; Lundqvist, B. I. *J. Phys.* **1971**, *4C*, 2064−2083.
(44) Blöchl, P. E.; Jepsen, O.; Andersen, O. K. *Phys. Rev.* **1994**, *B49*, 16 223−16 233.

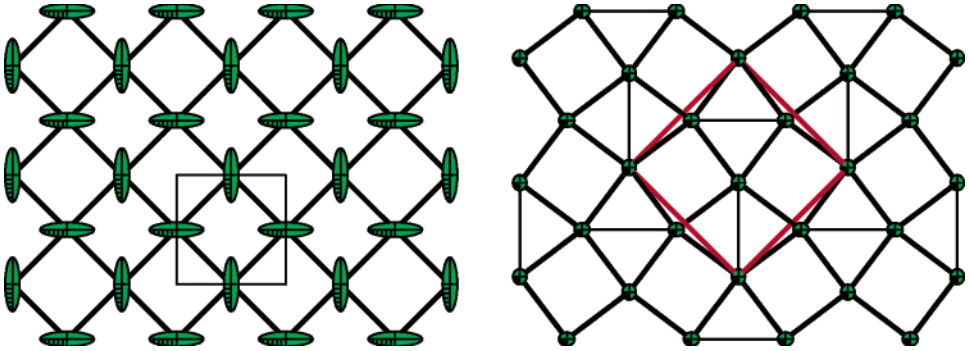

Figure 3. Planar net of Ti2 atoms (green). Left: undistorted; right: ordered model. Solid red lines denote the hypothetical $\sqrt{2} \times \sqrt{2} \times 1$ supercell.

the La_2Sb domain and the Cu_2Sb domain.[28] This structure map was developed after reflecting on the major structure determining factors for M_2Q pnictides and chalcogenides, which adopt more than 10 structure types with M being an early transition metal. Solid-state chemists familiar with metal-rich compounds know that higher valence-electron concentrations of M (vec_M), larger *d* orbitals of M (reflected in the principal quantum number n_M), and larger radius ratios r_M/r_Q, e.g., based on the Slater radii,[45] all tend to favor more M−M bonding. On the other hand, larger electron deficits of the Q atoms favor larger coordination numbers for the Q atoms, thus fewer M−M bonds, considering that the known structure types all have comparable packing efficiencies. The electron deficit of the Q atoms may be expressed as $(8 - e_Q)$, with e_Q = main group number of Q, in analogy to the $(8 - N)$ rule. Obviously these factors can compete against each other, one example being Zr_2S and Hf_2P that both form the Ta_2P type.[46] Subsequently we semiempirically derived the power product $\mathbf{f} = vec_M \times n_M^2 \times (r_M/r_Q)/(8 - e_Q)^2$, which yielded well defined domains by plotting **f** versus the averaged coordination number of the Q atoms.

The power product **f** may be calculated for all M_2Q binaries as well as $M_{1-\delta}M'_{1+\delta}Q$ and $M_2Q_{1-\delta}Q'_\delta$ ternaries, regardless of whether they are reported to exist or not. Thus, the structure type of unknown materials can be predicted, unless the compound in question either cannot be synthesized or forms a new type. Additionally, unlike longer established structure maps such as Pettifor's[47] or Villars',[48] this approach even suggests information about unknown types, namely the averaged coordination number of the Q atoms.

Thus far, the usability of this map was demonstrated in the subsequent uncoveries of new members of this M_2Q family, namely $Zr_{1-\delta}Ti_{1+\delta}As$,[29] $Zr_{1-\delta}V_{1+\delta}As$,[30] and HfMQ with M = Ti, V; Q = P, As.[31] Recently, the first example of a new type in this M_2Q family was detected, namely $Zr_2S_{0.33}Te_{0.67}$.[49] Its <C. N.(Q)> value is indeed eight, as rationalized by calculating its **f** value. Further, an extension to other stoichiometries is possible, as demonstrated by us for the M_5Q_3 compounds.[50,51]

In general, high coordination numbers of Q are reflected in small **f** values. Table 4 lists known and postulated examples with **f** < 10, all of which are predicted to have a coordination number of nine of the Q atoms, realized in tri-capped trigonal prismatic coordination. The structure of Ti_2Sb, the topic of this article, was foreseen to be either of the La_2Sb or Cu_2Sb type, for it occurs between the domains of these two types. Our experiments showed Ti_2Sb to crystallize in a distorted variant of La_2Sb, with the envisioned coordination number of nine for the Sb atoms.

Table 4. Overview of M_2Q Compounds with **f** < 10

compound	structure type	vec_M	n_M	r_M/Å	r_Q/Å	e_Q	f
ZrVP	Co_2Si	3.0	4.5	1.450	1.000	5	9.8
HfTiAs	Co_2Si	2.5	5.0	1.475	1.150	5	8.9
V_2P	Co_2Si	3.5	4.0	1.350	1.000	5	8.4
ZrTiP	Co_2Si	2.5	4.5	1.475	1.000	5	8.3
ZrVAs	La_2Sb	3.0	4.5	1.450	1.150	5	8.5
La_2Sb	La_2Sb	1.5	6.0	1.950	1.450	5	8.1
Zr_2Sb	La_2Sb	2.5	5.0	1.550	1.450	5	7.4
ZrTiAs	La_2Sb	2.5	4.5	1.475	1.150	5	7.2
Ti_2Sb	Ti_2Sb	2.5	4.0	1.400	1.450	5	4.3
Sc_2Sb	Cu_2Sb	1.5	4.0	1.600	1.450	5	2.9

Crystal Structure. The undistorted model of Ti_2Sb with its thermal ellipsoids is depicted in Figure 4, wherein we omitted the Ti−Sb bonds for clarity. The Ti atoms form corner-condensed Ti_6 (elongated) octahedra building planar layers parallel to the *a*,*b* plane by condensation of all vertexes of the basal plane formed by the Ti2 atoms. The Sb atoms reside above trigonal faces of the octahedra, forming eight Ti−Sb bonds within each layer. Furthermore, each Sb atom connects to an apex (Ti1) of a Ti_6 octahedron of the neighboring layer, which overall results in an Sb-centered tri-capped trigonal Ti_9 prism, and thus a truly three-dimensional structure.

In the (hypothetical) undistorted model, each basal $Ti2_4$ plane is a perfectly planar square, point group D_{4h}. This situation is realized in ZrTiAs, with Ti−Ti distances of 2.68 Å. That distance is enlarged in the binary antimonide, namely to 2.80 Å in the undistorted model. The bonds to the apexes of the tetragonally elongated "octahedron" of point group D_{4h} are 3.17 Å. The Ti−Ti distances in the plane are shorter than in elemental titanium (hexagonal closed packing, distances of 2.89 and 2.95 Å, respectively), which is indicative of strong Ti−Ti bonding. The structures of Ti_5Sb_3[33] and $Ti_{11}Sb_8$[52] are comprised of similar Ti−Ti bonds with lengths between 2.71 and 2.99 Å.

All bonding Ti−Sb distances are in the expected range, with values between 2.79 and 2.84 Å in the undistorted model. These compare well with the shortest Ti−Sb bonds found in other

(45) Slater, J. C. *J. Chem. Phys.* **1964**, *41*, 3199−3204.
(46) Villars, P. *Pearson's Handbook*, Desk Edition; American Society for Metals: Materials Park, OH, 1997.
(47) Pettifor, D. G. *Solid State Commun.* **1984**, *51*, 31−34.
(48) Villars, P. *J. Less-Comm. Met.* **1983**, *92*, 215−238.
(49) Örlygsson, G.; Conrad, M.; Harbrecht, B. *Z. Anorg. Allg. Chem.* **2001**, *627*, 1017−1022.
(50) Lee, C.-S.; Dashjav, E.; Kleinke, H. *J. Alloys Compd.* **2002**, *338*, 60−68.
(51) Derakhshan, S.; Dashjav, E.; Kleinke, H. *Mater. Res. Soc. Symp. Proc.* **2002**, *755*, 341−346.
(52) Bobev, S.; Kleinke, H. *Chem. Mater.* **2003**, *15*, 3523−3529.

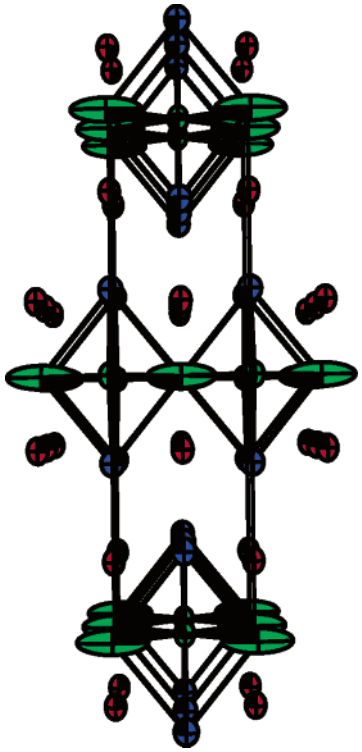

Figure 4. Crystal structure of (hypothetical) undistorted Ti_2Sb in a projection along the *a* axis (omitting Ti−Sb bonds for clarity). Blue: Ti1; green: Ti2; red: Sb. Vertical: *c* axis.

metal-rich Ti antimonides such as Ti_5Sb_3 (2.71 Å),[33] $Ti_{11}Sb_8$ (2.65 Å),[52] (Zr,Ti)Sb (2.85 Å)[53] and Ti_5SiSb_2 (2.71 Å).[54] Most of these bonds are of the order of the sum of Pauling's single bond radii of the elements:[55] $r_{Ti} + r_{Sb} = 1.32$ Å + 1.39 Å = 2.71 Å.

What changes result upon going from the undistorted model in the small unit cell to the distorted, experimentally observed one with the split position? The split position of Ti2 occurs with two physically impossible distances, namely the closest contact of 0.56 Å between two neighboring sites, and 2.40 Å as the next closest distance (cf. Pauling's single bond radius of 1.32 Å). The only one ordered pattern possible that (i) fills exactly every other position, and (ii) avoids both of the two unrealistic contacts, is displayed in the right part of Figure 3. The fact that no long-range order was detected by our diffraction experiments, is explained by the rather large distances between neighboring Ti2 layers, namely $c/2 = 7.31$ Å, and the absence of a direct connection of the two closest layers. Thus, the postulated ordered $\sqrt{2} \times \sqrt{2} \times 1$ superstructure is the smallest possible, with one Ti2 layer per primitive unit cell. Variations are only possible with regards to the stacking of the layers along the *c* axis.

In each distorted layer, the Ti2 atoms form a planar net comprising regular squares and equilateral rhombs both with edges of 2.82 Å, and the rhombs show diagonals of 3.40 and 4.51 Å, compared to 3.95 Å of the squares. In the hypothetical undistorted structure, the corresponding values are 2.80 Å for the edges, and 3.95 Å for the diagonals (the *a* lattice parameter). Alternatively one can describe the tessellation of the distorted

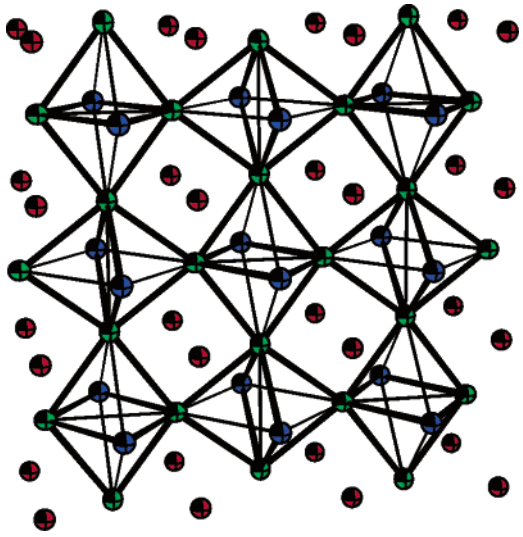

Figure 5. Layer of corner-sharing Ti_6 "octahedra" with surrounding Sb atoms in the ordered superstructure model. Blue: Ti1; green: Ti2; red: Sb. Bold Ti2−Ti2 bonds: 2.82 Å; thin Ti2−Ti2: 3.40 Å; bold Ti1−Ti2 bonds: 3.00 Å; thin: 3.35 Å.

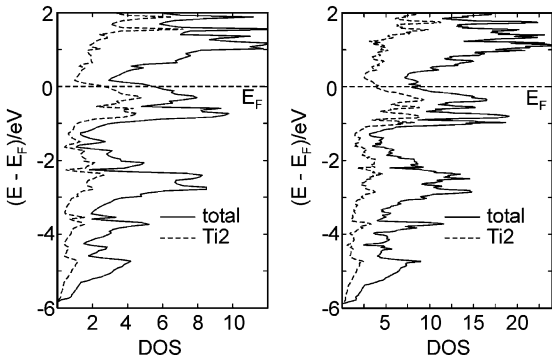

Figure 6. Densities of states of Ti_2Sb. Left: undistorted; right: superstructure model.

layer as a semi-regular 3^2434 net, treating each rhomb as two triangles. Topologically equivalent nets exist in the *secondary* tiling of, e.g., the U atoms of U_3Si_2,[56] the Zr atoms of $Zr_9Ni_2P_4$,[57] and the Sb chains of $(Zr,V)_{13}Sb_{10}$.[58] Figure 5 shows this solution with the surrounding Ti1 and Sb atoms. It is noted that the Sb atoms cap the $Ti2_4$ squares, and the Ti1 atoms the $Ti2_4$ rhombs. Therefore, the $Ti2_4$ squares of one layer are situated directly below the $Ti2_4$ rhombs of the next Ti2 layer, destroying the tetragonal symmetry.

The shortest Ti2−Sb bonds are only slightly affected by the distortion, with a small increase from 2.84 to 2.86 Å. On the other hand, the next-nearest Ti2−Sb distances change from 4.87 Å in the undistorted model quite significantly to 4.65 and 5.10 Å, as became evident in the experimental PDF data (see Figure 2). Moreover, the four equivalent Ti1−Ti2 distances from the apex to the basal plane of the octahedra (3.17 Å) are split into two distances of 3.00 Å and two of 3.35 Å. This reduces the point group of the Ti_6 "octahedra" from D_{4h} to D_{2h}.

Electronic Structure. The densities of states (DOS) of the undistorted model and of the smallest superstructure model are compared in Figure 6. Note that the states are given per eV

(53) Kleinke, H. *J. Am. Chem. Soc.* **2000**, *122*, 853−860.
(54) Kleinke, H. *Can. J. Chem.* **2001**, *79*, 1338−1343.
(55) Pauling, L. *The Nature of the Chemical Bond*, 3rd ed.; Cornell University Press: Ithaca, NY, 1948.
(56) Zachariasen, W. H. *Acta Crystallogr.* **1948**, *1*, 265−268.
(57) Kleinke, H.; Franzen, H. F. *Inorg. Chem.* **1996**, *35*, 5272−5277.
(58) Kleinke, H. *Chem. Commun. (Cambridge)* **1998**, 2219−2220.

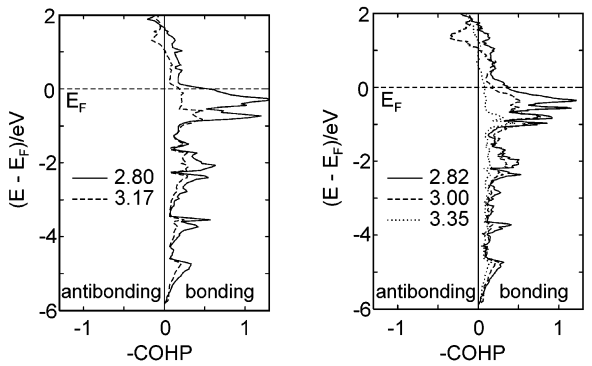

Figure 7. Selected Ti2−Ti2 (2.80 Å/2.82 Å) and Ti1−Ti2 (> 3.00 Å) crystal orbital Hamilton populations of Ti_2Sb. Left: undistorted; right: superstructure model.

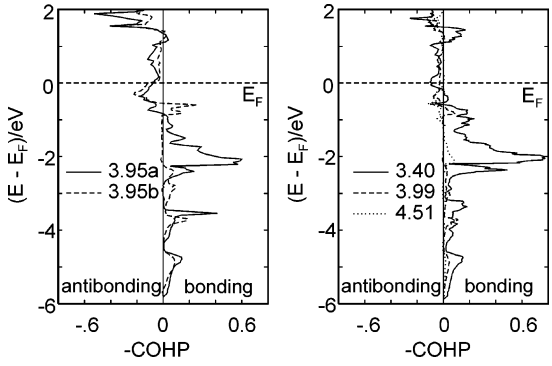

Figure 8. Selected Ti2−Ti2 crystal orbital Hamilton populations of Ti_2Sb. Left: undistorted; right: superstructure model.

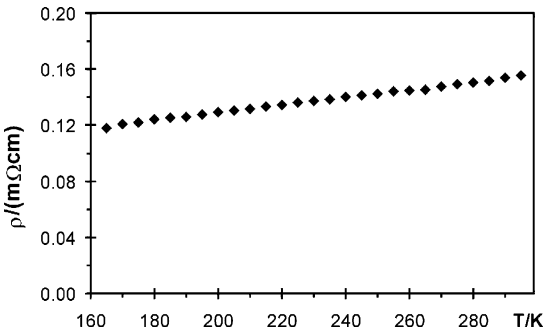

Figure 9. Specific electrical resistance of Ti_2Sb.

and cell, and that the superstructure has the cell doubled, which explains the higher numbers of the abscissa. As expected for such a metal-rich compound with numerous M−M bonds, Ti_2Sb is predicted to be metallic, regardless of the structure model considered. Although the overall shapes of the DOS curves are quite similar, the superstructure model obviously has a significantly smaller number of states per formula unit filled at the Fermi level (E_F), which occurs with a lower total energy (by 1.3 kJ/mol Ti_2Sb).

The dashed lines, corresponding to the Ti2 contributions, show that the smaller densities of states mainly stem from a different slope of the highest Ti2 peak under the Fermi level. To further analyze this peak, we investigate the Crystal Orbital Hamilton Populations (COHP curves)[59] of selected interactions involving Ti2. The averages of the shortest ones (<3.35 Å) are depicted in Figure 7, again with the undistorted model on the left and the superstructure on the right. In all of these interactions, in both models, only bonding states are filled. The Ti2−Ti2 COHP curve of 2.80 Å in the undistorted model shows two big peaks slightly below E_F that resemble the Ti2 peaks of the densities of states, and the Fermi level cuts through a shoulder of the upper peak. The highest filled peak of the corresponding bond in the superstructure (2.82 Å) exhibits a much smaller shoulder, which is the major Ti2 contribution to the DOS at E_F. Furthermore, it exhibits four peaks directly below E_F, instead of two. Overall, integrating over all filled states shows that these bonds are somewhat weaker than in the undistorted models, with integrated COHP values (ICOHPs) of −1.74 vs. −1.85 eV/bond (Table 3). Note that high negative values are indicative of strong bonding interactions.[60−62]

As noted before, the Ti1−Ti2 bonds of 3.17 Å in the undistorted model are split into 3.00 and 3.35 Å, respectively. The COHP curves indicate that in these cases, the number of filled bonding states correlate well with the bond lengths, i.e., the 3.00 Å bond is stronger, and the 3.35 Å bond weaker, than the 3.17 Å bond. This is reflected in the ICOHP values of −1.31 and −0.64 eV/bond in the superstructure (averaged −0.98 eV/bond) vs. −0.96 eV/bond in the undistorted model.

Here, the small gain in bond strength of the superstructure cannot make up for the loss in the short bonds of 2.80/2.82 Å. Therefore, the split of the Ti1−Ti2 distances cannot be the major driving force for the distortion. As the differences between the Ti2−Sb bonds of the two models are only marginal (Table 3), we turn our attention to the interactions along the diagonals of the squares and rhombs. In the undistorted structure, their lengths are 3.95 Å (the *a* and *b* axis), and we distinguish between two different ones. The first is capped by two Ti1 atoms (labeled 3.95a in the left part of Figure 8), and the second one by two Sb atoms (labeled 3.95b). Since Sb is more electronegative than Ti on any electronegativity scale, it pulls electron density away from the square. This results in a weaker, maybe negligible, interaction of −0.06, compared to −0.20 eV/bond for the diagonal capped by Ti1, a difference that is quite visible in the shape of the COHP curves.

The former interaction, capped by Sb atoms, remains virtually unchanged by going to the superstructure. While slightly larger (3.99 Å), its ICOHP value is the same (−0.06 eV/bond) in the superstructure. Rather drastic are the changes to the other square that is capped by two Ti1 atoms. Its two diagonals, equivalent in the undistorted La_2Sb type, are split to 3.40 and 4.51 Å, respectively. As the right part of Figure 8 illustrates, the interaction along the short diagonal of the $Ti2_4$ rhomb exhibits quite significant bonding character, with only a few antibonding states filled. For its ICOHP value is almost four times the value of the diagonal interaction in the undistorted square (−0.75 vs. −0.20 eV/bond), we identify the formation of this bond as the major driving force for the experimentally proven distortion.

Physical Properties. The experimentally determined specific electrical resistances are depicted in Figure 9. We observed the positive temperature dependence typical for metallic materials, as predicted for Ti_2Sb based on its computed band structure. The value at room temperature (0.16 mΩcm) is four times higher than that of elemental (metallic) titanium (0.04 mΩcm), which could be a result of the grain boundary effect.

(59) Dronskowski, R.; Blöchl, P. E. *J. Phys. Chem.* **1993**, *97*, 8617−8624.
(60) Landrum, G. A.; Dronskowski, R. *Angew. Chem., Int. Ed.* **2000**, *39*, 1560−1585.
(61) Elder, I.; Lee, C.-S.; Kleinke, H. *Inorg. Chem.* **2002**, *41*, 538−545.
(62) Dashjav, E.; Kleinke, H. *J. Solid State Chem.* **2003**, *176*, 329−337.

Conclusion

A new metallic binary antimonide, Ti_2Sb, was uncovered. Its most interesting structural feature is an unprecedented distortion of a metal atom layer that is a perfect square planar net in its aristotype La_2Sb. The corresponding Ti net of Ti_2Sb comprises squares and rhombs in a 1:1 ratio, as experimentally proven by X-ray structure studies and the pair distribution function technique based on both X-ray and neutron data, independent of the synthesis method applied. Electronic structure calculations indicate that the major driving force for the formation of the rhombs is enhanced Ti−Ti bonding along their diagonals.

A major difference to the more common square net distortions of main group examples (e.g., pnictides and chalcogenides), where the anionic components form the nets, is that the distortion results in more bonds per atom, not less, as the chalcogen nets typically distort to form two strong bonds in lieu of four weaker ones. Here an intermediate Ti−Ti bond was added while retaining the four short ones.

Furthermore, since even the single crystal structure refinements of the undistorted model yielded still reasonable residual factors (albeit suspicious thermal displacement parameters), other compounds reported to comprise square transition metal atom nets, in particular if studied only by means of powder diffraction, might exhibit the same distortion.

Acknowledgment. Financial support from NSERC, CFI, OIT (Ontario Distinguished Researcher Award for H.K.), the Province of Ontario (Premier's Research Excellence Award for H.K.) and the Canada Research Chair program (CRC for H.K.) is appreciated. S.J.B. would like to acknowledge funding from the NSF through grant DMR-0304391. PDF X-ray work was carried out at the MuCAT beamlines of the APS. The MuCAT sector is supported by the US-DOE through the Ames Laboratory under Contract No. W-7405-Eng-82. The APS is supported by the US-DOE under Contract No. W-31-109-Eng-38. Neutron PDF measurements were carried out at the NPDF beamline at Los Alamos Neutron Science Center (LANSCE). LANSCE is operated by the US-DOE under contract W-7405-ENG-36. The upgrade of NPDF was funded by NSF through grant DMR 00-76488. We would like to thank Hyun-Jeong Kim, Ahmad Masadeh, Thomas Proffen, Doug Robinson and Didier Wermeille for their help in collecting the PDF data, and the contributions of Pete Chupas, Clare Grey, Jon Hanson, and Peter Lee to the RAPDF technique developments.

Supporting Information Available: One X-ray crystallographic file (CIF), and one Figure displaying the experimental reduced structure function, $F(Q) = Q(S(Q) - 1)$, ((a) (X-ray) and (b) (neutron). This material is available free of charge via the Internet at http://pubs.acs.org.

JA048262E